

Experimental Identification of non-Abelian Topological Orders on a Quantum Simulator

Keren Li,^{1,2,*} Yidun Wan,^{3,4,*} Ling-Yan Hung,^{3,4,*} Tian Lan,⁴ Guilu Long,¹ Dawei Lu,^{2,†} Bei Zeng,^{2,5,6,‡} and Raymond Laflamme^{2,4,6}

¹State Key Laboratory of Low-Dimensional Quantum Physics and Department of Physics, Tsinghua University, Beijing 100084, China

²Institute for Quantum Computing and Department of Physics and Astronomy, University of Waterloo, Waterloo N2L 3G1, Ontario, Canada

³Department of Physics and Center for Field Theory and Particle Physics, Fudan University, Shanghai 200433, China

⁴Perimeter Institute for Theoretical Physics, Waterloo N2L 2Y5, Ontario, Canada

⁵Department of Mathematics & Statistics, University of Guelph, Guelph N1G 2W1, Ontario, Canada

⁶Canadian Institute for Advanced Research, Toronto M5G 1Z8, Ontario, Canada

Topological orders can be used as media for topological quantum computing — a promising quantum computation model due to its invulnerability against local errors. Conversely, a quantum simulator, often regarded as a quantum computing device for special purposes, also offers a way of characterizing topological orders. Here, we show how to identify distinct topological orders via measuring their modular S and T matrices. In particular, we employ a nuclear magnetic resonance quantum simulator to study the properties of three topologically ordered matter phases described by the string-net model with two string types, including the \mathbb{Z}_2 toric code, doubled semion, and doubled Fibonacci order. The third one, non-Abelian Fibonacci order is notably expected to be the simplest candidate for universal topological quantum computing. Our experiment serves as the basic module, built on which one can simulate braiding of non-Abelian anyons and ultimately topological quantum computation via the braiding, and thus provides a new approach of investigating topological orders using quantum computers.

PACS numbers: 11.15.-q, 71.10.-w, 05.30.Pr, 71.10.Hf, 02.10.Kn, 02.20.Uw

Introduction— Beyond the Landau-Ginzburg paradigm of symmetry breaking, topologically orders describe gapped quantum matter phases with a myriad of properties depending only on the topology but not of any microscopic details of the host system[1–5]. These properties are thus robust against local perturbations, where two of them are a finite set of degenerate ground states and a corresponding set of gapped (non-Abelian) anyon excitations[6, 7]. While the former may lead to a robust quantum memory[8], the latter may form a logical space that supports quantum computation via the unitary braiding of the anyons[6, 9–11]. This architecture of quantum computation is called topological quantum computation (TQC), because the ground states, anyons, and braiding operations are nonlocal by nature and hence are invulnerable against local errors. The most promising and simplest candidate topological order for universal TQC is the Fibonacci order[10, 11], which involves a non-Abelian anyon τ , and the braiding operations of two or more τ 's to form a universal set of unitary gates.

The potential, paramount applications of topological orders urges studies of topological orders in real systems. Rather than directly realizing a topological order in a real system, simulating it on a quantum computer offers an alternative means of investigating topological orders, where the first step is naturally to identify distinct topological orders. A topological order has three key features: topology-protected ground state degeneracy (GSD), finite number of anyon types, and topological properties of the anyons. As the first two characteristics are equivalent on a torus, distinguishing two topological orders can thus be achieved by comparing their GSDs or topological properties of the anyons. Particularly, the third characteristic, topological properties of the anyons, includes

the self-statistics, braiding, and fusion of the anyons. The self-statistics of an anyon can be a fraction, beyond the usual bosonic and fermionic statistics. The modular T matrix of a topological order, which in a proper basis is diagonal, records the self-statistics of all anyons in the topological order. The braiding of two anyons, namely one or multiple exchanges of two anyons, act on the state of the topological order with an observable effect that is captured by an observable—the S -matrix. Each element S_{ab} corresponds to the effect of a full exchange two anyons a and b . The fusion of two anyons is an interaction that produces other (not necessarily different) anyons in the topological order, which is also captured by the S matrix. Therefore, two distinct topological orders with the same ground state degeneracy can still be distinguished by comparing the modular T and S matrices[7, 12–15].

In this work, we consider the string-net model, also known as the Levin-Wen model[1], with only two string types. In this case, the model describes only three topological orders. The first two are the \mathbb{Z}_2 toric code and doubled semion order, which are Abelian topological orders. The third is the doubled Fibonacci order, which is non-Abelian and the candidate for universal TQC. As these three topological orders possess the same GSD on a torus, we need to identify them via their modular matrices. In experiment, we simulate each of the three topological orders on a nuclear magnetic resonance (NMR) quantum simulator [17–27], and measure its modular transformation ST^{-1} as a whole. As each of the three orders possess a unique ST^{-1} , we have thus identified all three topological orders of the string-net model in practice, and our experiment opens up a new way of identifying topological orders using quantum simulators.

String-net model— String-net models are exactly solvable,

infrared fixed point, effective models of topological orders in two spatial dimensions[1]. A string-net model is specified by a set of input data: string types $\{i, j, k, \dots\}$, fusion rules $\{N_{ij}^k \in \mathbb{Z}_{\geq 0}\}$, and Hamiltonian H , all defined on the honeycomb lattice (Fig. 1(a)). The strings are the fundamental degrees of freedom of the model, and each edge of the lattice has a unique string type, which can be changed by the Hamiltonian. For example, strings may be thought as spins living on the edges of the lattice. A fusion rule N_{ij}^k is defined on a vertex where the three incident edges of the string types i, j , and k , via the equation $i \times j = \sum_k N_{ij}^k k$, in which the non-negative integers N_{ij}^k are fusion coefficients. In this work, we deal with the cases where the strings are self-dual, i.e., $i = i^*$ for all string type i 's, and $N_{ij}^k \in \{0, 1\}$ only. The Hamiltonian of this model contains two parts

$$H = - \sum_v A_v - \sum_p B_p, \quad (1)$$

where the sums are respectively over all the vertices and plaquettes of the honeycomb lattice. A_v simply acts on a vertex; it returns unity if the three strings meeting at v satisfying a fusion rule and returns zero instead. B_p are highly nontrivial; hence, we will not elaborate on their precise forms until we introduce the three topological orders being simulated in this work. It turns out that all the A_v and B_p operators commute with each other, which renders the model exactly solvable. More importantly, all these operators are projectors, implying that their eigenvalues are either zero or one.

Given a set of input data of the string-net model, the degenerate ground states, anyon excitations, and modular T and S matrices form the set of output data, which characterizes a specific topological order based on the input data.

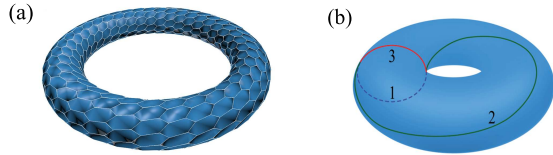


FIG. 1. (a) Honeycomb lattice on a torus. For the sake of ground states only, this can always be simplified into (b) The minimal honeycomb lattice on a torus: three edges (strings) labeled by 1, 2, and 3, two trivalent vertices, and one plaquette—the entire torus.

Minimal honeycomb lattice on a torus— Since the string-net model is an effective model at the infrared limit of certain microscopic theory of topological orders, the size of the lattice is irrelevant. In particular, on a torus, as far as ground states are concerned, one can always shrink the lattice to the minimal honeycomb lattice with merely three edges, two vertices, and one plaquette as shown in Fig. 1 by the F -moves[1, 2, 29] described in the supplemental material.

On the torus, the total Hilbert space is spanned by the basis states $|123\rangle$, where the numbers label both the edges and the string types carried respectively on the edges. These basis states are orthonormal: $\langle 1'2'3'|123\rangle = \delta_{1,1'}\delta_{2,2'}\delta_{3,3'}$. The

next step is to find the matrix form of the string-net Hamiltonian in Eq. (1) on this minimal honeycomb lattice. As we only concern about the ground states, we can set $A_v = 1$ at both vertices of the minimal lattice. The only nontrivial part of the Hamiltonian is thus B_p on the sole plaquette. We can derive (details in the supplemental material) that the matrix elements of B_p are

$$\begin{aligned} & \langle 1''2''3''|B_p|123\rangle \\ &= \frac{1}{D} \sum_{s,1',2',3'} d_s F_{s3'2'}^{123} F_{s1'3'}^{231} F_{s2''1'}^{3'12'} F_{s2'1''}^{3'1'2} F_{s1''3''}^{2''3'1'} F_{s3''2''}^{1''2'3'}. \end{aligned} \quad (2)$$

Here, the strings $1', 2'$, and $3'$ being summed over are those in the intermediate states, and s represents an average over all possible string types associated with the action of B_p . F_{klm}^{ijn} are the F -symbols, a collection of M^6 complex numbers determined by the fusion rules, for a case with M string types. In our setting, all F -symbols are real and $M = 2$. The total quantum dimension is $D = \sqrt{\sum_{i=0}^{M-1} d_i^2}$, where $d_i = F_{ii0}^{iii0}$ is defined as the quantum dimension of the string type i , and 0 is the trivial string type. A quantum dimension here is not the actual dimension of any Hilbert space but a convenient notation.

Technically, the F -symbols in Eq. (2) are a result of the associativity of the fusion of string types; hence they satisfy a consistency condition—the pentagon identity, as described in the supplemental material. The pentagon identity may possess multiple solutions. Each solution gives a set of F -symbols, which together with a set of previously defined input data of the string-net model, uniquely determines a set of output data, i.e., a topological order. Since the quantum dimensions d_i are defined by the F -symbol normalization, one may instead specify the quantum dimensions as part of a set of input data.

Three topological orders when $M = 2$ — Now we restrict ourselves to the cases that $M = 2$. In these cases, B_p is clearly an 8×8 real matrix, and so is the entire Hamiltonian. Due to the pentagon identity (see the supplemental material), for $M = 2$, there are three and only three possible sets of fusion rules, each of which gives rise to a string-net Hamiltonian describing a distinct topological order. Because $M = 2$, a string can precisely be simulated by a qubit. In the following, we only list the defining facts and topological properties of the three topological orders for $M = 2$ but leave certain details such as the matrix forms of the Hamiltonian to the supplemental material.

1. *\mathbb{Z}_2 toric code*. The input data includes: two string types 0 and 1, fusion rules $0 \times 1 = 1$ and $1 \times 1 = 0$, and quantum dimensions $d_0 = d_1 = 1$. The ground state space is four-dimensional on the torus, and the basis and corresponding modular T and S matrices are listed in Table. I. The four types of anyons are 1, e , m , and ϵ , where all are bosons except ϵ that is a fermion. The set of output data characterizes the \mathbb{Z}_2 toric code, which is an Abelian topological order.

2. *Doubled semion*. The input data set of this topological order differs from that of the \mathbb{Z}_2 toric code by $d_1 = -1$. The basis of the ground states, and T and S matrices are shown

Topo Orders	Anyons	Basis of the Ground States	Modular Matrices
\mathbb{Z}_2 toric code	$1 \quad e$ $m \quad \varepsilon$	$W_1 = (000\rangle + 011\rangle)/2, W_e = (000\rangle - 011\rangle)/2,$ $W_m = (101\rangle + 110\rangle)/2, W_\varepsilon = (101\rangle - 110\rangle)/2.$	$T = \text{Diag}\{1, 1, 1, -1\}$ $S = \frac{1}{2} \begin{pmatrix} 1 & 1 & 1 & 1 \\ 1 & 1 & -1 & -1 \\ 1 & -1 & 1 & -1 \\ 1 & -1 & -1 & 1 \end{pmatrix}$
Doubled semion	$1 \quad s$ $\bar{s} \quad s\bar{s}$	$W_1 = (000\rangle + 011\rangle)/2, W_s = (101\rangle + i 110\rangle)/2,$ $W_{\bar{s}} = (000\rangle - 011\rangle)/2, W_{s\bar{s}} = (101\rangle - i 110\rangle)/2.$	$T = \text{Diag}\{1, i, -i, 1\}$ $S = \frac{1}{2} \begin{pmatrix} 1 & 1 & 1 & 1 \\ 1 & -1 & 1 & -1 \\ 1 & 1 & -1 & -1 \\ 1 & -1 & -1 & 1 \end{pmatrix}$
Doubled Fibonacci	$1 \quad \tau$ $\bar{\tau} \quad \tau\bar{\tau}$	$W_1 = (000\rangle + 011\rangle)/\sqrt{5}\varphi,$ $W_\tau = (101\rangle + e^{-i\frac{4\pi}{5}} 110\rangle + \sqrt{\varphi}e^{i\frac{3\pi}{5}} 111\rangle)/\sqrt{5}\varphi,$ $W_{\bar{\tau}} = (101\rangle + e^{i\frac{4\pi}{5}} 110\rangle + \sqrt{\varphi}e^{-i\frac{3\pi}{5}} 111\rangle)/\sqrt{5}\varphi,$ $W_{\tau\bar{\tau}} = (\varphi^2 000\rangle - \varphi 011\rangle + \varphi^2 101\rangle + \varphi^2 110\rangle + \sqrt{\varphi} 111\rangle)/\sqrt{5}\varphi.$	$T = \text{Diag}\{1, e^{i\frac{4\pi}{5}}, e^{-i\frac{4\pi}{5}}, 1\}$ $S = \frac{1}{\sqrt{5}\varphi} \begin{pmatrix} 1 & \varphi & \varphi & \varphi^2 \\ \varphi & -1 & \varphi^2 & -\varphi \\ \varphi & \varphi^2 & -1 & -\varphi \\ \varphi^2 & -\varphi & -\varphi & 1 \end{pmatrix}$

TABLE I. Anyon types, the basis of the ground states, and modular matrices T and S for the three topological orders: \mathbb{Z}_2 toric code, doubled semion, and doubled Fibonacci, of the minimal honeycomb lattice on a torus. With respect to the T and S matrices, the rows and columns are in the order of the anyon types listed in the second column. For the non-Abelian doubled Fibonacci order, the parameter $\varphi = (1 + \sqrt{5})/2$, the golden ratio.

in Table. I. Here, the four types of anyons are 1 , s , \bar{s} , and $s\bar{s}$, among which s and \bar{s} are semions. A semion may be thought as a half fermion because its statistics is i instead of -1 . The set of output data characterizes the doubled semion order, which is also an Abelian topological order.

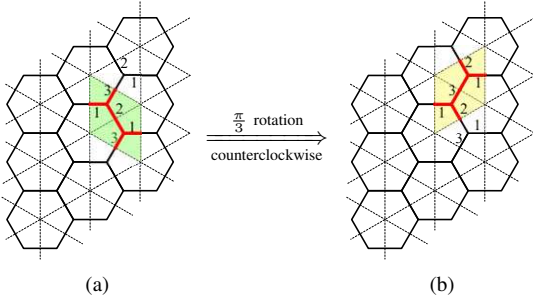


FIG. 2. (a) The honeycomb lattice with periodic boundary condition on the unit cell (green region) consisting of three edges 1, 2, and 3. This is in fact the minimal honeycomb lattice on a torus in Fig. 1. (b) The unit cell (yellow region) obtained from (a) by a $\pi/3$ rotation counterclockwise.

3. Doubled Fibonacci. We still have two string types 0 and 1, with, however, a new fusion rule $1 \times 1 = 0 \times 1$. This fusion rule leads to a different set of F -symbols, such that $d_0 = 1$ and $d_1 = \varphi = (1 + \sqrt{5})/2$, the golden ratio. The four degenerate ground states, and T and S matrices are shown in Table. I. The four types of anyons are 1 , τ , $\bar{\tau}$, and $\tau\bar{\tau}$, respectively. The anyon τ is called the Fibonacci anyon because the dimension of the Hilbert space of n τ 's grows as the Fibonacci sequence with n . The anyon $\bar{\tau}$ is the same as τ except that it has an opposite self-statistics. So, the anyon $\tau\bar{\tau}$ is a bound state of τ and $\bar{\tau}$. This is why the output topological order is called the doubled Fibonacci. The fusion of two Fibonacci anyons is $\tau \times \tau = 1 + \tau$; hence, the Hilbert space of two

Fibonacci anyons is two-dimensional and can be identified as the space of a logical qubit. The more Fibonacci anyons excited, the larger the logical space. The Fibonacci anyons are non-Abelian, whose braiding fabricates unitary quantum gates well suited for universal TQC [10, 11].

Experimental implementation—Our goal is to simulate the three topological orders above by 1) preparing their ground states, 2) performing the modular transformation on the virtual minimal honeycomb lattice, and 3) measuring the modular matrices that can uniquely distinguish the three topological orders. Here, we show how we would perform the modular transformations. It turns out that on the honeycomb lattice on a torus, T and S matrices cannot be simultaneously measured[30]; however, it is shown in [30] that a $\pi/3$ rotation of the lattice about the axis perpendicular to the lattice surface is equivalent to performing the combined modular transformation ST^{-1} . What crucial is that the three topological orders possess distinct matrices ST^{-1} and thus can be distinguished by measuring these matrices. Hence, we just need to know how a $\pi/3$ rotation acts on the ground states of a topological order. On a torus, a $\pi/3$ rotation transforms the minimal honeycomb lattice as depicted in Fig. 2. It is easy to see that the rotation cyclically permutes the three edges by $1 \rightarrow 2 \rightarrow 3 \rightarrow 1$. Consequently, the rotation transforms any state by $|e_1 e_2 e_3\rangle \rightarrow |e_3 e_1 e_2\rangle$, implying that one can then apply this permutation operation to the three bases of ground states and generate three new bases. Having done this, it is then straightforward to show that the inner product between the new and original bases reproduces the modular matrices ST^{-1} . In our experiment, the effect of the $\pi/3$ rotation, i.e., the cyclic permutation $1 \rightarrow 2 \rightarrow 3 \rightarrow 1$, is implemented by two SWAP gates, SWAP_{12} and SWAP_{23} .

Now we turn to our experimental procedure of identifying the three topological orders mentioned above. Our three-qubit system is represented by the ^{13}C -labeled trichloroethylene

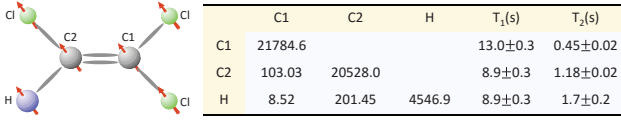


FIG. 3. Molecule structure of TCE, where one ^1H and two ^{13}C 's form a three-qubit system. The table on the right lists the parameters of chemical shifts (diagonal, Hz), J-coupling strengths (off-diagonal, Hz), and relaxation time scales T_1 and T_2 (second).

(TCE) molecule dissolved in d-chloroform [31]. The sample consists of two ^{13}C 's and one ^1H , with the structure shown in Fig. 3. All parameters of the molecule are listed in the table of Fig. 3, and all experiments were carried out on a Bruker DRX 700MHz spectrometer at room temperature.

Each experiment of simulating a given topological order was divided into three steps: 1) preparing its ground states, 2) performing the modular transformation which contains two SWAP gates, and 3) measuring the ground states before and after the modular transformation. Details can be found in the supplemental material.

1) Prepare the ground states. We first created a pseudo-pure state (PPS) [25, 32, 33] with the experimental fidelity over 0.99, and then prepared it into one of the ground states for \mathbb{Z}_2 toric code, doubled semion, and doubled Fibonacci order as shown in Table. I, respectively. These ground state preparation were all realized by the gradient ascent pulse engineering (GRAPE) optimizations [34, 35], with each pulse 10 ms. Denote each ground state of the currently simulated topological order as $|\phi_i\rangle$ ($1 \leq i \leq 4$).

2) Perform the modular transformation. For each of the four ground states $|\phi_i\rangle$, we applied two SWAP gates between qubit 1 and 2, and then qubit 2 and 3, to cyclically permutes the three qubits. They were optimized by GRAPE technique with pulse durations of 20 ms. It is equivalent to performing the modular transformations ($\pi/3$ rotation) on the torus of the minimal honeycomb lattice. Denote each new ground state of the currently simulated topological order as $|\psi_i\rangle$ ($1 \leq i \leq 4$).

3) Measure the ground states before and after the modular transformation. To acquire the ST^{-1} matrix in experiment, we need to calculate the inner products between the original and new ground states. A full state tomography was implemented before and after the modular transformations, to obtain the information of the original ground state $|\phi_i\rangle$ and new ground state $|\psi_i\rangle$, respectively.

Note that the state tomography inevitably leads to mixed states in experiment for the sake of experimental errors, say, ρ_i^{exp} for the original ground state and σ_i^{exp} for the new ground state were obtained after tomography. To calculate the inner products of the two states, it is necessary to purify ρ_i^{exp} and σ_i^{exp} to pure states. This step was realized by the maximum likelihood method [36], and $|\phi_i^{\text{exp}}\rangle$ and $|\psi_i^{\text{exp}}\rangle$ were found to be the closest to our experimental density matrices. As a result, each element in the experimentally reconstructed ST^{-1}

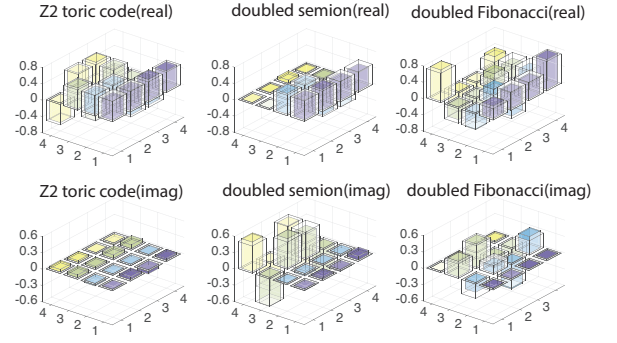


FIG. 4. ST^{-1} matrices for \mathbb{Z}_2 toric code, doubled semion, and doubled Fibonacci topological orders, respectively. The transparent columns represent the theoretical values, and the colored represent the experimental results.

matrix was

$$ST_{ij}^{-1} = \langle \phi_i^{\text{exp}} | \psi_j^{\text{exp}} \rangle, \quad (3)$$

from which the entire ST^{-1} could be reconstructed.

In Fig. 4, all the ST^{-1} matrices of the \mathbb{Z}_2 toric code, doubled semion and doubled Fibonacci topological orders are illustrated. The real parts of ST^{-1} are displayed in the upper row, and the imaginary in the lower row. In each figure, the transparent columns stand for the theoretical values, and the colored stand for the experimental results. From the figure, we conclude that our experiment matches well with the theoretical predictions, and each topological order is indeed identified clearly from its ST^{-1} matrix.

We also calculated the average fidelity [37] between the theoretical ST^{-1} matrix and the experimental one. For the non-Abelian doubled Fibonacci topological order, the average fidelity is 0.9825 ± 0.0048 , while for the other two Abelian topological orders \mathbb{Z}_2 toric code and doubled semion, the average fidelities are 0.9925 ± 0.0020 and 0.9918 ± 0.0027 , respectively. This provides another evidence that we have successfully identified distinct topological orders with high confidence using our quantum simulator.

Conclusion—Echoing the equivalence between the quantum circuit scheme and the topological quantum computation scheme, on a nuclear magnetic resonance quantum simulator, we successfully identify the doubled Fibonacci topological order, which is a promising candidate for topological quantum computation. Since the doubled Fibonacci order is one of the three topological orders described by the string-net model with two string types, using the same system, we also identify the other two topological orders, i.e., the \mathbb{Z}_2 toric code and the doubled semion. Our simulator can serve as a basic module for simulating the dynamical properties—in particular braiding and edge effects—of these topological orders.

We are grateful to the following funding sources: Industry Canada, NSERC and CIFAR (D.L., B.Z., and R.L.); National Natural Science Foundation of China under Grants No. 11175094 and No. 91221205 (K.L., and G.L.); National Basic

Research Program of China under Grant No. 2015CB921002 (K.L., and G.L.). YW thanks Lukasz Cincio, Yuting Hu, Chenjie Wang and Yang Qi for helpful discussions. YW is supported by the John Templeton foundation No. 39901. This research was supported in part by Perimeter Institute for Theoretical Physics. Research at Perimeter Institute is supported by the Government of Canada through the Department of Innovation, Science and Economic Development Canada and by the Province of Ontario through the Ministry of Research, Innovation and Science.

* These authors contributed equally to this work.

† d29lu@uwaterloo.ca

‡ zengb@uoguelph.ca

- [1] V. L. Ginzburg and L. D. Landau, *J. Exp. Theor. Phys.* **20**, 1064 (1950).
- [2] X.-G. Wen, F. Wilczek, and A. Zee, *Physical Review B* **39**, 11413 (1989), ISSN 0163-1829.
- [3] X.-G. Wen, *Int. J. Mod. Phys. B* **239** (1990).
- [4] X.-G. Wen and A. Zee, *Nuclear Physics B - Proceedings Supplements* **15**, 135 (1990), ISSN 09205632.
- [5] X. Chen, Z.-C. Gu, Z.-X. Liu, and X.-G. Wen, *Science (New York, N.Y.)* **338**, 1604 (2012), ISSN 1095-9203.
- [6] A. Kitaev, *Annals of Physics* **303**, 2 (2003), ISSN 00034916.
- [7] A. Kitaev, *Annals of Physics* **321**, 2 (2006), ISSN 00034916.
- [8] E. Dennis, A. Kitaev, A. Landahl, and J. Preskill, *Journal of Mathematical Physics* **43**, 4452 (2002), ISSN 00222488.
- [9] M. Freedman, A. Y. Kitaev, J. Preskill, and Z. Wang, *Bull. Amer. Math. Soc.* **40**, 31 (2003), ISSN 03029743, 0101025v2.
- [10] A. Stern and B. I. Halperin, *Physical Review Letters* **96**, 016802 (2006), ISSN 0031-9007.
- [11] C. Nayak, A. Stern, M. Freedman, and S. Das Sarma, *Reviews of Modern Physics* **80**, 1083 (2008), ISSN 0034-6861.
- [12] P. Bonderson, K. Shtengel, and J. K. Slingerland, *Physical Review Letters* **97**, 1 (2006), ISSN 00319007, 0601242.
- [13] P. Bonderson, A. Kitaev, and K. Shtengel, *Physical Review Letters* **96**, 1 (2006), ISSN 10797114, 0508616.
- [14] P. Bonderson, Ph.D. thesis, California Institute of Technology (2007).
- [15] E. Rowell, R. Stong, and Z. Wang, *Communications in Mathematical Physics* **292**, 343 (2009), ISSN 0010-3616.
- [1] M. Levin and X.-g. Wen, *Physical Review B* **71**, 21 (2005), ISSN 1098-0121, 0404617.
- [17] I. Buluta and F. Nori, *Science* **326**, 108 (2009).
- [18] I. M. Georgescu, S. Ashhab, and F. Nori, *Reviews of Modern Physics* **86**, 153 (2014).
- [19] S. Somaroo, C. H. Tseng, T. F. Havel, R. Laflamme, and D. G. Cory, *Physical review letters* **82**, 5381 (1999).
- [20] C. H. Tseng, S. Somaroo, Y. Sharf, E. Knill, R. Laflamme, T. F. Havel, and D. G. Cory, *Physical Review A* **61**, 12302 (1999).
- [21] X. Peng, J. Du, and D. Suter, *Physical Review A* **71**, 12307 (2005).
- [22] X. Peng, J. Zhang, J. Du, and D. Suter, *Physical review letters* **103**, 140501 (2009).
- [23] J. Du, N. Xu, X. Peng, P. Wang, S. Wu, and D. Lu, *Physical review letters* **104**, 30502 (2010).
- [24] G. A. Álvarez and D. Suter, *Physical Review Letters* **104**, 230403 (2010).
- [25] D. Lu, N. Xu, R. Xu, H. Chen, J. Gong, X. Peng, and J. Du, *Phys. Rev. Lett.* **107**, 20501 (2011).
- [26] Z. Li, H. Zhou, C. Ju, H. Chen, W. Zheng, D. Lu, X. Rong, C. Duan, X. Peng, and J. Du, *Physical review letters* **112**, 220501 (2014).
- [27] D. Lu, T. Xin, N. Yu, Z. Ji, J. Chen, G. Long, J. Baugh, X. Peng, B. Zeng, and R. Laflamme, *Physical Review Letters* **116**, 230501 (2016).
- [2] L.-Y. Hung and Y. Wan, *Physical Review B* **86**, 235132 (2012), ISSN 1098-0121, 1207.6169.
- [29] Y. Hu, S. Stirling, and Y.-s. Wu, *Physical Review B* **85**, 075107 (2012), arXiv:1105.5771v3.
- [30] L. Cincio and G. Vidal, *Physical Review Letters* **110**, 1 (2013), ISSN 00319007, 1208.2623.
- [31] D. Lu, A. Brodutch, J. Li, H. Li, and R. Laflamme, *New J. Phys.* **16**, 53015 (2014).
- [32] D. G. Cory, A. F. Fahmy, and T. F. Havel, *Proc. Natl. Acad. Sci. U.S.A.* **94**, 1634 (1997).
- [33] D. Lu, H. Li, D.-A. Trottier, J. Li, A. Brodutch, A. P. Krishnamanich, A. Ghavami, G. I. Dmitrienko, G. Long, J. Baugh, et al., *Phys. Rev. Lett.* **114**, 140505 (2015).
- [34] N. Khaneja, T. Reiss, C. Kehlet, T. Schulte-Herbrüggen, and S. J. Glaser, *J. Magn. Reson.* **172**, 296 (2005).
- [35] C. A. Ryan, C. Negrevergne, M. Laforest, E. Knill, and R. Laflamme, *Phys. Rev. A* **78**, 12328 (2008).
- [36] J. Reháček, Z. Hradil, and M. Ježek, *Physical Review A* **63**, 40303 (2001).
- [37] J. Emerson, R. Alicki, and K. Życzkowski, *Journal of Optics B: Quantum and Semiclassical Optics* **7**, S347 (2005).

Certain details of the String-net model with two string types

Meaning of F -symbols

In the set of input data of the string-net model, fusion rules of the input string types comprise a key element. The following discussion is formally described by the language of unitary fusion categories; however, so as to be self-contained and clear to broader audience, we shall not use the formal language but explain things in plain words.

The fusion rules are associative in the following sense. Since $i \times j$ for two string types i and j in general produces more than one string types, $i \times j$ is regarded as a multi-dimensional vector space—called a fusion space—taking a string type as a vector. The associativity of fusion means the fusion-space isomorphism $(i \times j) \times k \cong i \times (j \times k)$. This isomorphism implies that a unitary, linear transformation between the two fusion spaces $(i \times j) \times k$ and $i \times (j \times k)$. Canonically, we can denote a basis state of $(i \times j) \times k$ by $v_{ij}^m v_{mk}^l$, meaning that i and j fuse into a particular string type m , which then fuses with k and yields a particular string type l . Note that m is not summed over. It is illustrative to regard i, j , and k as the input string types, m the internal string type, and l the output string type. With this setting, the associativity reads

$$v_{ij}^m v_{mk}^l = \sum_n F_{jkn}^{ilm} v_{il}^n v_{jk}^n, \quad (4)$$

which defines the F -symbols as the coefficients in the linear superposition on the RHS. This relation is also called an F -move. Note that here we neglected certain subtleties in the notation of the basis states for simplicity, which does not impact the point we are addressing. A full account of the associativity and F -symbols can be easily found in the literature, e.g., Ref.[1, 2]. From the associativity (4), one sees that F_{jkn}^{ilm} vanishes unless $N_{ij}^m \neq 0$, $N_{kl}^m \neq 0$, $N_{il}^n \neq 0$, and $N_{jk}^n \neq 0$.

When considering fusing four and more string types, there is a vector space due to each possible order of fusing these string types, and all such fusion spaces with fixed input and output string types are isomorphic. These isomorphisms impose further consistency conditions on the F -symbols. It turns out that the fusion spaces involving four input string types suffice to yield a consistency condition that determines the isomorphisms between fusion spaces of any higher dimensions. This consistency condition is the pentagon identity:

$$\sum_n F_{kpn}^{mlq} F_{mns}^{jip} F_{lkr}^{jns} = F_{qkr}^{jip} F_{mls}^{riq}. \quad (5)$$

Legitimate F -symbols have to be solutions to the pentagon identity. To uniquely specify the string-net model, apart from the set of input data described in the main text, a solution to the pentagon identity is also necessary.

String-net Hamiltonian on the minimal honeycomb lattice on a torus

As introduced in the main text, the string-net Hamiltonian consists of two types of operators, vertex/charge operators A_v acting on vertices v and plaquette/flux operators B_p acting on plaquettes p of the honeycomb lattice. The operators A_v are merely δ -functions in our consideration and are thus neglected from our discussion. The operators B_p are nontrivial. Generally, a B_p is a weighed average as follows.

$$B_p = \frac{1}{D} \sum_s d_s B_p^s, \quad (6)$$

where d_s is the quantum dimension of string type s , and D the total quantum dimension of all input string types. Here, B_p^s is a flux operator with a definite string type s ; its action on a plaquette p inserts a loop of string type s within the plaquette p along the boundary of p . Via the F -moves (4), the type- s string loop can be dissolved into the boundary edges of the plaquette p and hence modify the string types on these edges. Since p has six boundary edges/vertices, this procedure of dissolving the string loop yields six F -symbols[1, 2]. One can choose to start the procedure at any vertex and continue in any direction along p 's boundary. The result is independent of the choice. By choosing to begin with the vertex where the edges e_1 , e_6 , and l_1 meet and go counterclockwise, we obtain the following action of B_p^s on p .

$$B_p^s \left| \begin{array}{c} \text{Diagram of a hexagonal plaquette } p \text{ with boundary edges } e_1, e_2, e_3, e_4, e_5, e_6 \text{ and vertices } l_1, l_2, l_3, l_4, l_5, l_6 \end{array} \right\rangle = \sum_{e'_a} F_{se'_6e'_1}^{l_1e_1e_6} F_{se'_1e'_2}^{l_2e_2e_1} F_{se'_2e'_3}^{l_3e_3e_2} \times \\ F_{se'_3e'_4}^{l_4e_4e_3} F_{se'_4e'_5}^{l_5e_5e_4} F_{se'_5e'_6}^{l_6e_6e_5} \left| \begin{array}{c} \text{Diagram of the same hexagonal plaquette } p \text{ with modified boundary edges } e'_1, e'_2, e'_3, e'_4, e'_5, e'_6 \end{array} \right\rangle, \quad (7)$$

where the summation runs over all primed string types e'_1 through e'_6 , collectively denoted by e'_a . Clearly, only the string types on the boundary edges of p are altered. The question now is the form of the B_p^s (7) on the minimal honeycomb lattice on a torus. Bearing in mind that the minimal lattice here has only one plaquette, with however three boundary edges, because of the periodic boundary condition. So, there is certain repetition of the three edges, such that they can bound a hexagonal plaquette. Staring at the unit cell before applying the periodic boundary condition in Fig. 1(a) in the main text, repeated here as Fig. 5(a), one can see that the lattice divides the unit cell into three regions p_1 , p_2 , and p_3 . These three regions can be viewed as three incomplete plaquettes, which

will form a single complete plaquette p (Fig. 5(b)) under periodic boundary condition.

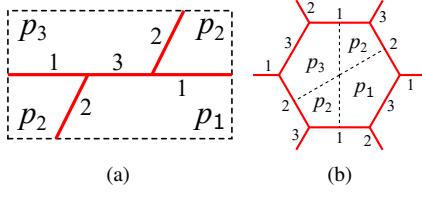


FIG. 5. (a) The unit cell that forms the minimal honeycomb lattice on a torus after applying periodic boundary condition. There are three incomplete plaquettes virtually. (b) The single plaquette formed by the unit cell due to periodic boundary condition.

Therefore, we can simply apply the B_p^s (7) to the plaquette in Fig. 5(b) in the following manner. We apply the B_p^s (7) to each of the virtual, incomplete plaquettes p_1 through p_3 by choosing a starting one and an order. Do this at one virtual plaquette all at once, that is, each time taking two F -symbols from the B_p^s (7) corresponding to the virtual plaquette being acted on. This procedure would be done in two steps with caution. First, on the plaquette Fig. 5(b), boundary edges are simultaneously external edges too; however, a B_p^s action would not change the external edges. So, when acting a B_p^s on a virtual plaquette, say, p_1 for example, one should keep the external-edge indices 1 and 2 in the corresponding F -symbols unaltered but changing the boundary-edge indices 1, 3, and 2 to primed indices in the F -symbols. Second, having done so on one virtual plaquette, say, again p_1 , the change of the boundary-edge indices should propagate to the remaining external edges that have the same indices as those of the boundary edges of p_1 . Then repeat the two steps on the next virtual plaquette and so on. Keep in mind that there is actually merely one plaquette; hence, we have only one weighing factor d_s/D in averaging B_p^s with different string types s to make B_p . In the end, we obtain

$$B_p |123\rangle = \frac{1}{D} \sum_{s,1',2',3'} d_s F_{s3'2'}^{123} F_{s1'3'}^{231} F_{s2'1'}^{3'12'} \times F_{s2'1'}^{3'1'2} F_{s1'3''}^{2''3'1'} F_{s3''2''}^{1''2'3''} |1''2''3''\rangle. \quad (8)$$

The matrix elements of B_p in the main text are thus just the inner product between the RHS of the expression above and $\langle 1''2''3''|$.

The job now is to substitute in Eq. (8) the F -symbols corresponding to each set of the input data with two string types to get the numerical form of the B_p operator and thus of the Hamiltonian. We list in the equation below the relevant non-vanishing F -symbols.

$$\mathbb{Z}_2 \text{ spin liquid : } F = 1, \quad (9)$$

$$\text{Doubled semion : } F = 1 \text{ except } F_{110}^{110} = -1, \quad (10)$$

$$\text{Doubled Fibonacci : } F_{11n}^{11m} = \begin{pmatrix} \phi^{-1} & \phi^{-\frac{1}{2}} \\ \phi^{-\frac{1}{2}} & -\phi^{-1} \end{pmatrix}, \quad (11)$$

where in the last line, the matrix is understood as indexed by $m, n \in \{0, 1\}$. We can then write down the numeric forms of the B_p matrix in the three cases above. In order to simulate the Hamiltonian, we would better expand the B_p matrices in terms of the Pauli matrices acting on the three edges (qubits) respectively. Because the \mathbb{Z}_2 spin liquid and doubled semion both have rather trivial F -symbols, their Hamiltonians are rather trivial too. Hence, we only show in below the Pauli-matrix-decomposed string-net Hamiltonian of the doubled Fibonacci order on the minimal honeycomb lattice on the torus. The operators appearing in this decomposition are $\sigma_i \otimes \sigma_j \otimes \sigma_k$, where the three Pauli matrices act respectively on the three qubits 1, 2, and 3. The subscripts $i, j, k = \{0, x, y, z\}$ label the corresponding Pauli matrices, and $\sigma_0 = \mathbb{1}$ is understood. We denote the corresponding coefficients of these terms by c_{ijk} . As such, formally the doubled Fibonacci Hamiltonian would read

$$H_{\text{dF}} = \sum_{i,j,k} c_{ijk} \sigma_i \otimes \sigma_j \otimes \sigma_k. \quad (12)$$

Many such coefficients vanish actually; hence, we only list the nonvanishing coefficients as follows.

$$\begin{aligned} c_{000} &= \frac{2\sqrt{5}+5}{40}, \quad c_{00x} = -\frac{2\sqrt{2}}{(\sqrt{5}+1)^{\frac{5}{2}}(\sqrt{5}+5)}, \\ c_{00y} &= \frac{2-\sqrt{5}}{8}, \quad c_{0x0} = \frac{\sqrt{2}(\sqrt{5}-1)}{(\sqrt{5}+1)^{\frac{5}{2}}(\sqrt{5}+5)}, \\ c_{0xx} &= \frac{3}{8} - \frac{1}{2\sqrt{5}}, \quad c_{0xy} = -c_{00x}, \quad c_{0xz} = -\frac{i}{8}, \\ c_{0y0} &= \frac{1}{2} - \frac{9}{8\sqrt{5}}, \quad c_{0yx} = -c_{00x}, \quad c_{0yy} = \frac{6\sqrt{5}-5}{40}, \\ c_{0zx} &= -i\frac{4\sqrt{5}-15}{40}, \quad c_{0zy} = -\frac{i\sqrt{2}}{(\sqrt{5}+1)^{\frac{3}{2}}(\sqrt{5}+5)}, \\ c_{0zz} &= \frac{1}{8}, \quad c_{x00} = c_{00x}, \quad c_{x0x} = \frac{3}{8} - \frac{3}{4\sqrt{5}}, \\ c_{x0y} &= -c_{00x}, \quad c_{x0z} = \frac{i}{8}, \quad c_{x0x} = c_{0xx}, \\ c_{xxy} &= \frac{2\sqrt{5}-5}{40}, \quad c_{xy0} = -c_{00x}, \\ c_{xyx} &= \frac{3(2\sqrt{5}-5)}{40}, \quad c_{xyy} = c_{00x}, \quad c_{xyz} = -\frac{i}{8}, \\ c_{xz0} &= -\frac{i(5\sqrt{5}+3)}{8(3\sqrt{5}+5)}, \quad c_{xzy} = \frac{i(\sqrt{5}-1)}{8(3\sqrt{5}+5)}, \\ c_{y00} &= c_{00y}, \quad c_{y0x} = -c_{00x}, \quad c_{y0y} = \frac{4\sqrt{5}-5}{40}, \\ c_{yx0} &= -c_{00x}, \quad c_{yxx} = \frac{2\sqrt{5}-5}{40}, \\ c_{yxy} &= -\frac{\sqrt{2}(\sqrt{5}+3)}{(\sqrt{5}+1)^{\frac{5}{2}}(\sqrt{5}+5)}, \\ c_{yxz} &= \frac{i}{8}, \quad c_{yy0} = c_{0yy}, \quad c_{yyx} = c_{00x}, \end{aligned} \quad (13)$$

$$\begin{aligned}
c_{yyy} &= \frac{1}{4} - \frac{7}{8\sqrt{5}}, c_{yz0} = -c_{0zy}, c_{yzx} = i\frac{2\sqrt{5}-5}{40}, \\
c_{yzz} &= c_{zyz} = c_{zzy} = -\frac{1}{8}, c_{z0x} = c_{zxy} = -\frac{i}{8}, \\
c_{z0z} &= c_{zz0} = c_{0zz}, c_{zx0} = c_{zyx} = c_{x0z}.
\end{aligned}$$

Ground states of the string-net model with two string types

In general, it is not easy to find the ground-state basis of the string-net Hamiltonian, in which the modular T matrix is diagonal, such that each basis state is associated with a non-contractible Wilson loop with a well-defined flux going through. One way of doing this is to resort to the loop operators defined in Ref.[1], which is rather involved. On the minimal honeycomb lattice on a torus, however, there is a handy method— Q -algebra[3], which can give us solutions immediately. An introduction to Q -algebra is beyond the scope of this supplemental material. The ground states we obtain using this method are presented in the main text. It is then straightforward to verify that the ground states we find are indeed the ground states of the corresponding Hamiltonians.

Experimental procedure

As shown in Fig. 6, an experiment for a given topological order simulation was divided into three steps: 1) preparing its ground states, 2) performing the modular transformation which contains two SWAP gates, and 3) measuring the ground states before and after the modular transformation.

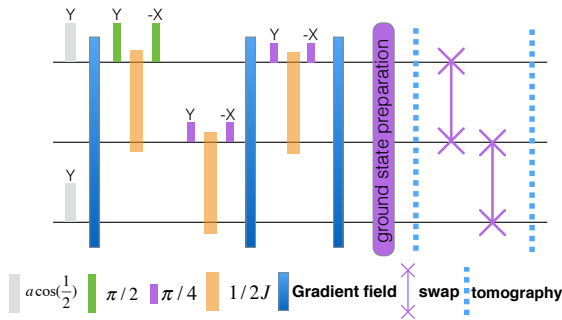


FIG. 6. Sequence of the NMR Experiment. It includes three parts: preparing the ground states, performing the modular transformation which contains two SWAP gates, and measuring the ground states via full state tomography before and after the modular transformation. The sequence before the ground state preparation denoted by the purple block is used to create the pseudo-pure state.

Preparation of the pseudo-pure state

In our three-qubit NMR system, the thermal equilibrium state ρ_{eq} is,

$$\rho_{eq} = \frac{1-\epsilon}{8}\mathbb{I} + \epsilon(\gamma_H\sigma_z^1 + \gamma_C\sigma_z^2 + \gamma_C\sigma_z^3), \quad (14)$$

where $\epsilon \approx 10^{-5}$ describes the polarization, \mathbb{I} is a 8×8 identity matrix, and γ_H and γ_C are the gyromagnetic ratios of the ^1H and ^{13}C nuclei, respectively. As the identity part does not influence the unitary operations or measurements in NMR experiments, the original density matrix of ρ_{eq} can be replaced by the deviation one for simplicity. Since $\gamma_H \approx \gamma_C$,

$$\rho_{eq} = 4\sigma_z^1 + \sigma_z^2 + \sigma_z^3. \quad (15)$$

To create the pseudo-pure state

$$\rho_{000} = \frac{1-\epsilon}{8}\mathbb{I} + \epsilon|000\rangle\langle 000|, \quad (16)$$

we used the spatial average technique as shown by the pulse sequence before the ground state preparation in Fig. 6, which include three z -gradient fields. In between any two gradient fields, we packed the pulses into three GRAPE pulses. The entire procedure of the pseudo-pure state creation takes about 15ms with the simulated fidelity 99.8%. In experiment, the fidelity is around 99%.

Experimental results of the prepared ground states

Realized by 10 ms GRAPE optimization pulses, the prepared ground states $|\phi_i\rangle$ ($1 \leq i \leq 4$) for \mathbb{Z}_2 toric code, doubled semion, and doubled Fibonacci order, are reconstructed respectively. Table II summarizes all of the fidelities for the found states.

	$ \phi_1\rangle$	$ \phi_2\rangle$	$ \phi_3\rangle$	$ \phi_4\rangle$
\mathbb{Z}_2 toric code	0.9751	0.9866	0.9803	0.9827
Doubled semion	0.9877	0.9750	0.9821	0.9729
Doubled fibonacci	0.9723	0.9746	0.9894	0.9705

TABLE II. Fidelities of the experimentally prepared ground states.

Experimental ST^{-1} matrix

After the modular transformation, the elements in ST^{-1} are obtained via $ST_{exp}^{-1}(i, j) = \langle \phi_i^{exp} | \psi_j^{exp} \rangle$. We list all the experimental ST^{-1} matrices here, where ST_z^{-1} denotes \mathbb{Z}_2 toric code, ST_s^{-1} denotes doubled semion, and ST_f^{-1} denotes the doubled fibonacci topological order, respectively.

$$ST_z^{-1} = \begin{pmatrix} 0.4562 - 0.0069i & 0.4735 - 0.0455i & 0.5114 + 0.0520i & -0.4830 + 0.0466i \\ 0.4808 + 0.0449i & 0.4943 - 0.0234i & -0.5237 + 0.0311i & 0.4950 + 0.0312i \\ 0.5251 - 0.0734i & -0.4882 - 0.0304i & 0.4967 + 0.0641i & 0.5227 - 0.0079i \\ 0.4988 + 0.0303i & -0.4788 - 0.0140i & -0.4613 + 0.0708i & -0.5051 - 0.0440i \end{pmatrix} \quad (17)$$

$$ST_s^{-1} = \begin{pmatrix} 0.4916 - 0.0318i & 0.5074 - 0.0103i & -0.0067 - 0.5320i & -0.0065 + 0.5449i \\ 0.5092 + 0.0280i & 0.4960 - 0.0468i & 0.0001 + 0.5351i & 0.0127 - 0.4504i \\ 0.4546 - 0.0341i & -0.5017 - 0.0108i & 0.0097 + 0.4352i & 0.0790 + 0.4866i \\ 0.4384 + 0.0648i & -0.5269 - 0.0435i & 0.0308 - 0.4656i & 0.0189 - 0.5207i \end{pmatrix} \quad (18)$$

$$ST_f^{-1} = \begin{pmatrix} 0.3042 - 0.0010i & -0.4138 - 0.1784i & -0.3111 + 0.2846i & 0.7667 - 0.0001i \\ 0.3919 - 0.0050i & 0.3330 + 0.1110i & -0.6265 + 0.4288i & -0.3847 + 0.0263i \\ 0.4015 + 0.0043i & -0.5594 - 0.4744i & 0.3388 - 0.1109i & -0.3756 - 0.0209i \\ 0.7360 + 0.0107i & 0.2821 + 0.3109i & 0.2602 - 0.2822i & 0.3786 + 0.0209i \end{pmatrix} \quad (19)$$

Meanwhile, for comparison, the theoretical matrix are presented:

$$ST_z^{-1} = \begin{pmatrix} 0.5 & 0.5 & 0.5 & -0.5 \\ 0.5 & 0.5 & -0.5 & 0.5 \\ 0.5 & -0.5 & 0.5 & 0.5 \\ 0.5 & -0.5 & -0.5 & -0.5 \end{pmatrix} \quad (20)$$

$$ST_s^{-1} = \begin{pmatrix} 0.5 & 0.5 & -0.5i & 0.5i \\ 0.5 & 0.5 & 0.5i & -0.5i \\ 0.5 & -0.5 & 0.5i & 0.5i \\ 0.5 & -0.5 & -0.5i & -0.5i \end{pmatrix} \quad (21)$$

$$ST_f^{-1} = \begin{pmatrix} 0.2764 & -0.3618 - 0.2629i & -0.3618 + 0.2629i & 0.7236 \\ 0.4472 & 0.2236 + 0.1625i & -0.5854 + 0.4253i & -0.4472 \\ 0.4472 & -0.5854 - 0.4253i & 0.2236 - 0.1625i & -0.4472 \\ 0.7236 & 0.3618 + 0.2629i & 0.3618 - 0.2629i & 0.2764 \end{pmatrix} \quad (22)$$

To describe how closely that experimental ST^{-1} matrix approximates the theoretical ones, we used the average fidelity defined by

$$\bar{F}(\Lambda, \mathcal{U}) = \int \langle \psi | \mathcal{U}^\dagger \Lambda (|\psi\rangle\langle\psi|) \mathcal{U} | \psi \rangle d\mu(\psi) \quad (23)$$

where Λ is our measured ST^{-1} matrix, \mathcal{U} is the theoretical ST^{-1} matrix which is unitary, and $d\mu(\psi)$ is the unitarily invariant distribution of pure states known as Fubini-Study measure. We randomly sampled 1000 $|\psi\rangle$'s from the two-qubit pure state space, and replace the integral in Eq. (23) by the sum (with some normalization). The calculated average fidelities for all three topological orders are shown in Table III.

To get the uncertainty, we repeat this random sampling procedure for 100 times. The average fidelity and uncertainty are

defined as the mean and standard deviation of the 100 repetitions, respectively.

* These authors contributed equally to this work.

† d29lu@uwaterloo.ca

‡ zengb@uoguelph.ca

[1] M. Levin and X.-g. Wen, Physical Review B **71**, 21 (2005), ISSN 1098-0121, 0404617, URL <http://arxiv.org/abs/cond-mat/0404617><http://link.aps.org/doi/10.1103/PhysRevB.71.045110>.

[2] L.-Y. Hung and Y. Wan, Physical Review B **86**, 235132 (2012), ISSN 1098-0121, 1207.6169.

	Z_2 spin liquid	Doubled Semion	Doubled Fibonacci
$\bar{F}(\Lambda, \mathcal{U})$	0.9925 ± 0.0020	0.9918 ± 0.0027	0.9825 ± 0.0048

TABLE III. Average fidelities of the experimental ST^{-1} matrices compared to the theoretical results for all three topological orders. To get the uncertainty, we repeat this random sampling procedure for 100 times, while in each sampling 1000 two-qubit pure states are randomly chosen. The average fidelity and uncertainty are defined as the mean and standard deviation of the 100 repetitions, respectively.

- [3] T. Lan and X. G. Wen, Physical Review B - Condensed Matter and Materials Physics **90**, 1 (2014), ISSN 1550235X, 1311.1784.